Received Date : 15-Sep-2014
Revised Date : 19-Dec-2014
Accepted Date : 05-Jan-2015
Article type : Research Article

The pyrazolobenzothiazine core as a new chemotype of p38 alpha mitogen-activated protein kinase inhibitors

Stefano Sabatini[1], Giuseppe Manfroni[1,*], Maria Letizia Barreca[1,*], Silke M. Bauer[2], Marco Gargaro[3], Rolando Cannalire[1], Andrea Astolfi[1], Jose Brea[4], Carmine Vacca[3], Matteo Pirro[5], Serena Massari[1],Oriana Tabarrini[1], Maria Isabel Loza[4], Francesca Fallarino[3], Stefan A. Laufer[2], and Violetta Cecchetti[1]

1 Department of Pharmaceutical Sciences, University of Perugia, Via A. Fabretti, 48, 06123 Perugia (Italy)
2 Department of Pharmaceutical & Medicinal Chemistry, Institute of Pharmacy, Eberhard-Karls University Tuebingen, Auf der Morgenstelle 8, 72076 Tuebingen (Germany).
3 Department of Experimental Medicine, University of Perugia, Piazzale Gambuli, 06100 Perugia (Italy)
4 CIMUS Research Center, University of Santiago de Compostela, Avda de Barcelona s/n, Planta 3. Despacho 1, 15782 Santiago de Compostela (Spain)
5 Department of Medicine, University of Perugia, Piazzale Gambuli, 06100 Perugia (Italy)

corresponding authors: giuseppe.manfroni@unipg.it, marialetizia.barreca@unipg.it

Abstract: The identification, synthesis, biological activity and binding mode prediction of a series of pyrazolobenzothiazines as novel p38α MAPK inhibitors are reported. Some of these compounds showed interesting activity in both p38α MAPK and TNF-α release assays. Derivative **6** emerged as the most interesting compound with IC_{50} (p38α) = 0.457 μM, IC_{50} (TNF-α) = 0.5 μM and a promising kinase selectivity profile. The obtained results strongly indicate the pyrazolobenzothiazine core as a new p38α inhibitor chemotype worthy of future chemical optimization efforts directed toward identifying a new generation of anti-inflammatory agents.

This article has been accepted for publication and undergone full peer review but has not been through the copyediting, typesetting, pagination and proofreading process which may lead to differences between this version and the Version of Record. Please cite this article as an 'Accepted Article', doi: 10.1111/cbdd.12516

Keywords: pyrazolobenzothiazines; p38α MAPK inhibitors; anti-TNF agents; molecular docking; ligand efficiency.

Introduction

p38 Mitogen-activated protein kinases (MAPKs) are a class of evolutionary conserved serine/threonine kinases that link extracellular signals to the intracellular machinery modulating a plethora of cellular processes (*e.g.* cell cycle, cell death, differentiation, and senescence) (1-4). It is well known that p38 MAPKs play an essential role in regulating the production of cytokines as tumor necrosis factor alpha (TNF-α), interleukins 1β and 6 which in turn represent the major mediators in inflammatory autoimmune diseases such as rheumatoid arthritis, psoriasis, lupus erythematosus, bowel diseases, asthma, chronic obstructive pulmonary disease (COPD), and type-1 diabetes (2-4). More recently, some other consolidated roles of p38 MAPKs in the pathogenesis of Parkinson's disease (5), multiple sclerosis (6,7), cancer (8-10), and Alzheimer's disease (11,12) are emerging from literature data. There are four isoforms of p38 MAPK (α, β, γ, δ also called MAPK14, MAPK11, MAPK12, MAPK13, respectively) that are encoded by separate genes and show ≥ 60% overall sequence similarity and >90% identity in catalytic domain (13,14). The four isoforms have different tissue distribution with p38α MAPK and, to less extent, p38β MAPK being ubiquitous. The latters are overexpressed during the activation of the inflammatory process and regulate TNF-α and cytokines production (1,2,13,14) designating p38α MAPK a valid target for therapeutic intervention (15).

In the past two decades, tremendous efforts have been made by both pharmaceutical companies and academic groups to identify and develop new potent and selective p38α MAPK inhibitors, some of which have reached different stage of clinical trials. Furthermore, their mechanisms of action, kinase selectivity, crystallographic and computational studies, and pharmacological profiles have been extensively reviewed in literature (15-21). Notwithstanding these promising results, multiple attempts to generate clinically useful p38α MAPK inhibitors have generally failed, either due to toxicity or inadequate efficacy. However, several first generation p38α MAPK inhibitors are still in clinical trials for asthma, COPD, neuropathic pain, etc (22).

Particular interest has been recently focused on the identification of a new generation of p38α MAPK inhibitors able to overcome both the low *in vivo* efficacy and safety. Toward this direction, many pharmaceutical companies have recently filed several patents reporting the discovery and potential clinical use of new potent molecules especially devoted to the treatment of asthma or COPD (23). In parallel, the identification of new chemotypes able to inhibit p38α MAPK function is of a great relevance.

In this context, we herein describe the identification of a novel class of p38α MAPK inhibitors. In the past, some of us reported that the pyrazolobenzothiazine core proved to be a promising scaffold for anti-inflammatory activity, although at that time it was not possible to investigate the mechanism of action (24). With this history as backdrop, a series of 34 pyrazolobenzothiazines (**1**-**6**, Scheme 1, 2 and Table 1) was subsequently designed and synthesized by merging the structures of meloxicam and celecoxib in the search of selective inhibitors of cycloxygenase isoform two (COX-2). Unfortunately, when tested for their ability to inhibit the prostaglandin E_2 (PGE_2) production in a biochemical assay employing both COX-1 and COX-2 isoenzymes, all compounds resulted inactive (data not shown). Anyway, we felt confident enough about the potentiality of the pyrazolobenzothiazine scaffold for anti-inflammatory activity to decide to test series **1-6** against another target well-known to be involved in the inflammatory process, that is p38α MAPK. This target selection was also supported by a somehow structural similarity between our compounds and **SB203580** (25-29), one of the best studied p38α MAPK inhibitors. Taking into account the bioisosteric relationship between the imidazole (**SB203580**) and the pyrazole (in house compounds) nucleus, two chemical similarity hypothesis could be proposed depending on the functionalization at the N-1 atom in the pyrazolobenzothiazine scaffold (Figure 1). The main difference between the two assumptions consisted in the pyrazolobenzothiazine functional group corresponding to the *para*-pyridinyl substituent of the known inhibitor. In derivatives **1**-**3**, the phenyl ring of the benzothiazine core replaced the pyridine moiety of **SB203580** whilst in derivatives **4-6** we focused the attention on the hydrogen-bond acceptor character of the pyridinyl nitrogen atom, which could be mimicked by the sulfone group.

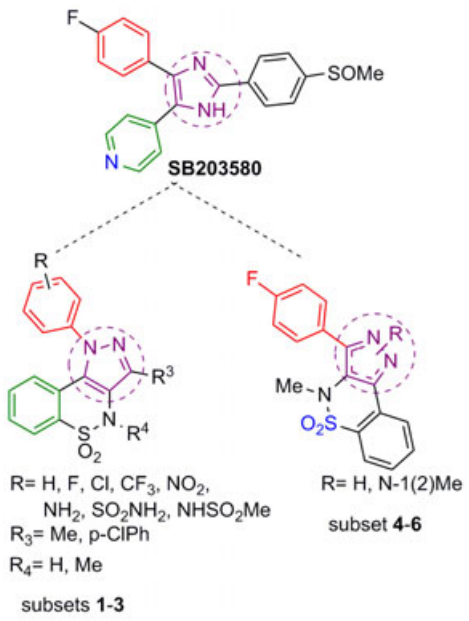

Figure 1. General structure of pyrazolobenzothiazines **1**-**6** and **SB203580**. Keeping constant the pyrazole ring as bioisosteric replacer of imidazole ring of **SB203580,** two chemical similarities hypothesis are proposed. The different colours highlight the chemical similarities between the two chemotypes.

In this paper, we report the synthesis, the biological evaluation, the structure-activity relationship (SAR) and computational studies of pyrazolobenzothiazine derivatives **1**-**6**.

Material and Methods

General Chemistry

All starting materials were commercially available, unless otherwise indicated. Reagents and solvents were purchased from common commercial suppliers and were used as such. Organic solutions were dried over anhydrous Na_2SO_4 and evaporated to dryness with a rotary evaporator at low pressure. All reactions were routinely checked by thin-layer chromatography (TLC) on silica gel 60F254 (Merck) and visualized by using UV or iodine. Column chromatography separations were carried out on Merck silica gel 60 (mesh 70-230), flash chromatography on Merck silica gel 60 (mesh 230-400). Melting points were determined in capillary tubes (Büchi Electrotermal model 9100) and are uncorrected. Yields were of purified products and were not optimized. The reactions conducted under microwaves irradiation were carried out employing a microwave reactor Biotage Initiator^{TM} 2.0 version 2.3 build 6250. Ultrasonic mediated reactions were carried out in VWR Ultrasonic Bath (HF45kHz80W) made by VWR, Malaysa. ^{1}H NMR spectra were recorded at 200 or 400 MHz (BrukerAvance DRX-200 or 400, respectively) while ^{13}C NMR spectra were recorded at 100 MHz (BrukerAvance DRX-400). Chemical shifts are given in ppm (δ) relative to TMS. Spectra were acquired at 298 K. Data processing was performed with standard Bruker software XwinNMR and the spectral data are consistent with the assigned structures. All compounds were ≥95% pure as determined by LC/MS using an Agilent 1290 Infinity System machine equipped with DAD detector from 190 to 640 nm. With exception of derivative **5**, that was analyzed at 254±4 nm, the purity was revealed at 270.4±4 nm**.** For compounds **1a**-**k**, **2a**-**k**, **3a**-**c**, **3f**-**k**, **4**, and **6** an Phenomenex AerisWIDEPORE C18 (2.1 mm × 100 mm, 1.7 µm particle size column) reverse phase was used with gradient of 0-100% acetonitrile with 0.1% formic acid (channel B) in water with 0.1% formic acid (channel A) for 20 min. at 0.3 mL/min. Injection volume was 0.5 µL and column temperature of 40 °C. Peaks retention time are given in minutes. Compound **5** was instead analyzed using an Phenomenex AerisWIDEPORE C4 All-ion (4.6 mm × 100 mm, 3.6 µm particle size column) employing the same parameters as used for previous compounds. Detection was based on electrospray

ionization (ESI) in negative polarity using Agilent 1290 Infinity System equipped with a MS detector Agilent 6540UHD Accurate Mass Q-TOF.

General Procedure for Preparation of Pyrazolobenzothiazes 1a-i (Method A). In a microwave oven tube, the key synthon **7** (30) (1 mmol) was dissolved in DMF (2.5 mL) and the appropriate phenylhydrazine hydrochloride (1.5 mmol) was added. The solution was irradiated at 100 °C from 5 to 75 min, employing the following experimental parameters: pressure 5 bar, cooling on, FHT on, prestirring 30 s, very high absorption. The solution was then poured into ice-water and acidified with 2N HCl (pH = 4) to give a precipitate which was filtered, dried and crystallized by EtOH.

Experimental details and analytical data for compounds **1a**-**i** are reported in Supporting Information.

[4-(3-methyl-5,5-dioxidopyrazolo[4,3-c][1,2]benzothiazin-1(4H)-yl)phenyl]amine (1j). A stirred solution of the nitro derivative **1i** (0.52 g, 1.4 mmol) in DMF (30 mL), was hydrogenated over catalytic amount of Raney nickel at room temperatuere and atmospheric pressure for 30 min. The mixture was filtered over Celite and the filtrate was evaporated to dryness; the residue was crystallized by EtOH to give target amino derivative **1j** (0.30 g, 65%) as pale brown solid: mp 287-288 °C. ^{1}H NMR (200 MHz, DMSO-d_6): δ 2.25 (s, 3H, CH_3), 5.80 (brs, 2H, NH_2), 6.70-6.80 (m, 2H, H-3' and H-5'), 6.90-7.25 (m, 3H, H-9, H-2', and H-6'), 7.45-7.70 (m, 2H, H-7 and H-8), 7.75-8.00 (m, 1H, H-6), 10.25 (brs, 1H, NH). HRMS (ESI) *m/z* $[M+H]^+$ calcd for $C_{16}H_{14}N_4O_2S$: 327.0910, found: 327.0916; LC-MS: ret. time 6.44 min.

In a similar manner, compound **2j** was prepared starting from **2i** (See Supporting Information)

N-*[4-(3-methyl-5,5-dioxidopyrazolo[4,3-c][1,2]benzothiazin-1(4H)-yl)phenyl]methanesulfonamide (1k).* To a solution of compound **1j** (0.3 g, 0.92 mmol) in a 1:1 dry CH_2Cl_2/pyridine mixture (50 mL) and under nitrogen flux, methanesulfonyl chloride (0.4 mL, 4.5 mmol) was added dropwise at 0 °C. The mixture was then stirred at 50 °C for 24h and the solvent was concentrated to one third of the volume. Water was added and the mixture was acidified with 2N HCl (pH=3) and extracted with EtOAc (5 times). The organic phases were collected and washed with brine, dried and evaporated to dryness. The crude residue was purified by flash column chromatography eluting with CH_2Cl_2/MeOH (95:5) to give target compound **1k** (0.20 g, 54%) as pale brown solid: mp 298-300 °C. ^{1}H NMR (200 MHz, DMSO-d_6): δ 2.30 (s, 3H, CH_3), 3.15 (s, 3H, SO_2CH_3), 6.95-7.05 (m, 1H, H-9), 7.30-7.70 (m, 6H, H-7, H-8, H-2', H-3', H-5', and H-6'), 7.95-8.00 (m, 1H, H-6), 10.25 (brs, 1H,

SO_2NH), 10.55 (brs, 1H, benzothiazine SO_2NH). HRMS (ESI) *m/z* $[M+H]^+$ calcd for $C_{17}H_{16}N_4O_4S_2$: 405.0692, found: 405.0686; LC-MS: ret. time 7.66 min.

In a similar manner, compound **2k** was prepared starting from **2j** (See Supporting Information)

General Procedure for the Preparation of Compounds 2b-g and 2i. Method B. To a suspension of 60% NaH (2.5 mmol) in dry DMF (3 mL) cooled at 0 °C and under nitrogen flux, a solution of the appropriate compound (**1b-g** and **1i**) (1 mmol) in dry DMF (5 mL), was added dropwise. After 30 min, MeI (0.62 mL, 10 mmol) diluted in dry DMF (1 mL), was added dropwise and the mixture was stirred for additional 1h at room temperature. The mixture was then poured into ice/water and extracted several time with EtOAc, the combined organic layers were washed with brine and dried. The crude residue was purified as reported below for each compound to give the target derivatives **2b**-**g** and **2i**.

Experimental details and analytical data for compounds **2b-g** and **2i** are reported in Supporting Information.

4-(3,4-Dimethyl-5,5-dioxidopyrazolo[4,3-c][1,2]benzothiazin-1(4H)-yl)benzenesulfonamide (2h). To a suspension of K_2CO_3 (0.021 g, 0.15 mmol) in dry DMF (1 mL), a solution of compound **1h** (0.060 g, 0.15 mmol) in dry DMF (3 mL) was added dropwise and the mixture was stirred at room temperature for 1h. MeI (0.011 mL, 0.17 mmol) diluted in dry DMF (1 mL) was then added dropwise and the mixture was stirred at room temperature for 15h. The mixture was poured into ice/water and the formed precipitated was filtered to give a solid which was crystallized by MeOH to give compound **2h** (0.054 g, 89%) as white solid: mp 275-276 °C. ^{1}H NMR (200 MHz, $CDCl_3$): δ 2.45 (s, 3H, CH_3), 3.15 (s, 3H, NCH_3), 4.95 (s, 2H, SO_2NH_2), 7.10 (dd, *J* = 1.2 and 7.4 Hz, 1H, H-9), 7.40-7.65 (m, 2H, H-7 and H-8), 7.70 (m, 2H, H-2' and H-6'), 7.95-8.10 (m, 3H, H-6, H-3' and H-5'). HRMS (ESI) *m/z* $[M+H]^+$ calcd for $C_{17}H_{16}N_4O_4S_2$: 405.0692, found: 405.0687; LC-MS: ret. time 8.87 min.

2-[2-(4-Fluorophenyl)-2-oxoethyl]-1,2-benzisothiazol-3(2H)-one 1,1-dioxide (8) (31)***.*** To a solution of saccharin sodium salt (9.40 g, 46 mmol) in dry DMSO (30 mL) a solution of 2-bromo-1-(4-fluorophenyl)ethanone (5.00 g, 23.0 mmol) in dry DMSO (10 mL) was added dropwise and the reaction was stirred at 70 °C for 3h. The mixture was then poured into ice/water to give a precipitate which was filtered to give **8** (6.50 g, 88%) as crude product which was used as is in the next reaction step: mp 177-178 °C. ^{1}H NMR (200 MHz, DMSO-d_6): δ 5.45 (s, 2H, CH_2), 7.25-7.45 (m, 2H, H-3' and H-5'), 7.90-8.20 (m, 5H, H-5, H-6, H-7, H-2', and H-6'), 8.30 (d, *J* = 8.1 Hz, 1H, H-4).

(4-Fluorophenyl)(4-hydroxy-1,1-dioxido-2H-1,2-benzothiazin-3-yl)methanone (9) (31)**.** Shiny metallic sodium (0.60 g, 26 mmol) was added to absolute EtOH (80 mL), the mixture was stirred at room temperature until the sodium was completely dissolved. Then, a dried powder of intermediate **8** (3.30 g, 10.3 mmol) was added at once and the red solution was stirred at 60 °C for 1h. The mixture was poured into ice/water and slowly acidified with 12N HCl (pH = 2) obtaining a precipitate that was filtered to give compound **9** (2.60 g, 78%) as yellow crude solid which was used as is in the next reaction step: mp 188-189 °C. ^{1}H NMR (200 MHz, DMSO-d_6): δ 7.30-7.50 (m, 2H, H-3' and H-5'), 7.80-7.95 (m, 3H, H-5, H-6, and H-7), 8.00-8.25 (m, 3H, H-8, H-2', and H-6'), 9.90 (brs, 1H, NH).

3-(4-Fluorophenyl)-1,4-dimethyl-1,4-dihydropyrazolo[4,3-c][1,2]benzothiazine 5,5-dioxide (4) *and* ***3-(4-Fluorophenyl)-2,4-dimethyl-2,4-dihydropyrazolo[4,3-c][1,2]benzothiazine 5,5-dioxide (5).*** In a microwave oven tube, the benzothiazinone **9** (0.60 g, 1.9 mmol) was dissolved in EtOH (10 mL) and methylhydrazine (0.30 mL, 5.7 mmol) was added. The solution was irradiated at 100 °C for 30 min, employing the following experimental parameters: pressure 5 bar, cooling on, FHT on, prestirring 30 s, very high absorption. The solvent was distilled off and the residue was chromatographed eluting with $CHCl_3$/MeOH (99:1) in order to remove impurities. A 1:1 mixture (0.4 g) of regioisomers 3-(4-fluorophenyl)-1-methyl-1,4-dihydropyrazolo[4,3-*c*][1,2]benzothiazine 5,5-dioxide (**10**) and 3-(4-fluorophenyl)-2-methyl-2,4-dihydropyrazolo[4,3-*c*][1,2]benzothiazine 5,5-dioxide (**11**) was obtained and dissolved in dry DMF (7.0 mL). This solution was added dropwise to a stirred suspension of 60% NaH (0.12 g, 3.03 mmol) in dry DMF (2 mL) at 0 °C. The mixture was kept at 0 °C under stirring for additional 30 min. The MeI (0.75 mL, 12.1 mmol) diluted in dry DMF (2.0 mL) was added dropwise and the mixture was stirred at room temperature for 1h then poured into ice/water and extracted with EtOAc (3 times). The combined organic layers were washed with brine, dried and filtered. The solvent was removed under vacuum to give a crude product formed by the two methylated regioisomers **4** and **5**. After flash chromatographic separation eluting with cyclohexane/EtOAc (50:50) the N-1 methyl regioisomer **4** (R_f< by TLC) (0.04 g) and the N-2 methyl regioisomer **5** (R_f> by TLC) (0.07 g) were obtained as white solids. A fraction of the two regioisomers enriched by compound **4** was further crystallized by MeOH to give additional 0.07 g of **4**.

Compound **4** (0.11 g, 52%): mp 217-219 °C. ^{1}H NMR (400 MHz, DMSO-d_6): δ 2.85 (s, 3H, N-4 CH_3), 4.30 (s, 3H, N-1 CH_3), 7.30-7.40 (m, 2H, H-3' and H-5'), 7.80 (t, J = 7.6 Hz, 1H, H-7), 7.90-8.05 (m, 4H, H-6, H-8, H-2', and H-6'), 8.10 (d, J = 7.8 Hz, 1H, H-9). ^{13}C NMR (100 MHz, DMSO-d_6): δ 38.83, 40.65, 116.47 (d, $J_{C\text{-}F}$ = 22.0 Hz, C-3' and C-5'), 122.46, 124.23, 125.59, 125.90, 127.93 (d, $J_{C\text{-}F}$ = 3.0 Hz, C-1'), 128.23 (d, $J_{C\text{-}F}$ = 8.2 Hz, C-2' and C-6'), 130.23, 130.39, 130.65, 134.06, 140.85, 172.45 (d, $J_{C\text{-}F}$ = 140.0 Hz, C-4'). 2D ^{1}H NMR

NOESY spectra showed two relevant NOE cross-peaks: N-1 CH_3→H-9; N-1 CH_3→H-8. HRMS (ESI) *m/z* [*M*+H]$^+$ calcd for $C_{17}H_{14}FN_3O_2S$: 344.0870, found: 344.0863; LC-MS: ret. time 11.93 min.

Compound **5** (0.07 g, 33%): mp 212-215 °C. ^{1}H NMR (400 MHz, DMSO-d_6): δ 2.80 (s, 3H, N-4 CH_3), 3.90 (s, 3H, N-2 CH_3), 7.25-7.55 (m, 2H, H-3' and H-5'), 7.65-7.75 (m, 3H, H-7, H-2', H-6'), 7.85 (t, J = 7.5 Hz, 1H, H-8), 7.90 (d, J = 7.8 Hz, 1H, H-6), 8.10 (d, J = 7.6 Hz, 1H, H-9). ^{13}C NMR (100 MHz, DMSO-d_6): δ 38.82, 39.37, 116.80 (d, $J_{C\text{-}F}$ = 22.0 Hz, C-3' and C-5'), 123.09, 123.88, 123.92, 124.74, 128.02, 129.68, 131.84, 131.95 (d, $J_{C\text{-}F}$ = 9.0 Hz, C-2' and C-6'), 133.96, 135, 74, 136.73, 165.04 (d, $J_{C\text{-}F}$ = 140.0 Hz, C-4'). HRMS (ESI) *m/z* [*M*+H]$^+$ calcd for $C_{17}H_{14}FN_3O_2S$: 344.0870, found: 344.0867; LC-MS: ret. time 12.08 min.

(4-Fluorophenyl)(4-hydroxy-2-methyl-1,1-dioxido-2H-1,2-benzothiazin-3-yl)methanone (12). A mixture of intermediate **9** (0.39 g, 1.2 mmol) in 1N NaOH/EtOH (1:4) (10 mL) was stirred at room temperature untill a red solution was obtained. Then, MeI (0.23 mL, 3.7 mmol) was added dropwise and the solution was stirred for 3h at room temperature and after diluted with 0.5 N HCl (20 mL) giving a precipitate which was filtered and dried. Compound **12** was obtained (0.33 g, 82%) as yellow solid and used as is for the next reacion step: mp 161-163 °C. ^{1}H NMR (200 MHz, DMSO-d_6): δ 2.70 (s, 3H, CH_3), 7.40-7.55 (m, 2H, H-3' and H-5'), 7.90-8.05 (m, 3H, H-5, H-6, and H-7), 8.10-8.25 (m, 3H, H-8, H-2', and H-6').

3-(4-Fluorophenyl)-4-methyl-1,4-dihydropyrazolo[4,3-c][1,2]benzothiazine 5,5-dioxide (6). In neat conditions compound **12** (0.37 g, 1.1 mmol) and hydrazine monohydrate (0.27 mL, 5.5 mmol) were heated at 70 °C under sonication for 20 min. The excess of hydrazine monohydrate was removed under vaccum distillation and the residue was poured into ice/water and acidified with 2N HCl (pH=3) to give an orange precipitate which was filtered, dried and purified by flash column chromatogrphy eluting with $CHCl_3$/MeOH (99:1) to give derivative **6** (0.20 g, 55%), as pale yellow solid: mp 195-197 °C. ^{1}H NMR (200 MHz, DMSO-d_6): δ 2.80 (s, 3H, CH_3), 7.40-7.50 (m, 2H, H-3' and H-5'), 7.60-8.10 (m, 6H, H-6, H-7, H-8, H-9, H-2', and H-6'). HRMS (ESI) *m/z* [*M*+H]$^+$ calcd for $C_{16}H_{12}FN_3O_2S$: 330.0713, found: 330.0707; LC-MS: ret. time 10.62 min.

Biological assays

p38α MAPK assay (32) and human whole blood (HWB) assay (33) were performed following a procedure previously reported. Experimental details of the two methods employed are reported in the Supporting Information.

The kinase functional assays were performed in 384-well plates using a 30 µL reaction volume. The reactions were run in reaction buffer. The reaction was initiated by combination of kinase (Carna Biosciences) and 1.5 µM peptide substrate in the presence of ATP. The reaction mixture was analyzed on the Caliper EZ Reader (Perkin Elmer) by the electrophoretic mobility shift of the fluorescent substrate and phosphorylated product. Inhibition data were calculated by comparison to no enzyme control reactions for 100% inhibition and DMSO-only reactions for 0% inhibition. Dose-response curves were generated to determine the concentration required to inhibit 50% of kinase activity (IC50). Staurosporine was included as a positive control of each enzymatic assay. Compounds **1d** and **6** were also evaluated with this method on p38α MAPK yielding to an IC_{50} value of 0.31 µM and 1.9 µM, respectively, consistent with data reported in Table 2.
The concrete conditions for each enzymatic reactions are reported in the Supporting Information (Table S1).

Computational methods

Docking studies were performed using the software AutoDock 4.2 (AD4.2) (34). The crystal structure of p38α MAPK complexed with inhibitor **SB203580** (PDB code 3ZS5) (35) was retrieved from the RCSB Protein Data Bank and used as target structure for our modeling studies.

Before the docking run, the complex was submitted to Schrödinger's Protein Preparation Wizard (36,37): water molecules were deleted, hydrogen atoms were added, bond orders and charges were then assigned, the orientation of hydroxyl groups on Ser, Thr and Tyr, the side chains of Asn and Gln residues, and the protonation state of His residues were optimized. The inhibitor **SB203580** was then extracted from the complex and its coordinates were transformed in order to exclude any biasing toward the experimental protein-bound conformation.

Pyrazolobenzothiazine derivatives **1d**, **1k**, **2d**, **2k**, **3k** and **6** were built using the Schrödinger Maestro Interface (38) and then submitted to Polak–Ribiere conjugate gradient minimization [0.0005 kJ/(Å mol) convergence].

Prior to docking, particular attention was directed to the ionization state of the sulfonamide nitrogen of derivatives **1d**, **1k** and **3k**, and the possible tautomeric state of the pyrazole ring in derivative **6**. These inhibitors were thus processed by MoKa (39,40), a software able to accurately predict pKa values and tautomerism in the aqueous medium. The in silico analysis indicated pKa values of 4.64 (**1d** and **1k**) and 4.16 (**3k**) for the sulfonamide group; at pH=7-7.5, this moiety thus exists only in the anionic form (98% abundance). Therefore,

we considered the sulfonamide moiety of compounds **1d**, **1k** and **3k** as bearing negatively charged nitrogen. Furthermore, the ligand pyrazole moiety of **6** was predicted to exist in solution as an equilibrium between two tautomeric forms (1H- and 2H-pyrazole), which were both taken in consideration for the computational study.

Ligands and receptor structures were converted to AD4 format files using AutoDockTools (41), and then the Gesteiger–Marsili partial charges were then assigned. The dimensions of the grid were 60 × 60 × 60 with grid points separated by a 0.375 Å. The grid was centered on the ATP binding site, using the **SB203580** crystallographic position as reference. The Lamarckian genetic algorithm local search method was used, and for each compound the docking simulation was composed of 100 runs. Clustering of docked conformations was performed on the basis of their root-mean-square deviation (rmsd) (tolerance = 2.0 Å), and the results were ranked based on the estimated free energy of binding. The cluster analysis revealed a predominant ligand orientation for all studied compounds (89, 74, 74, 51, 74, 100 and 67 conformations in the first ranked cluster for **1d**, **1k**, **2d**, **2k**, **3k**, and 1H- and 2H-pyrazole tautomers of **6,** respectively), and the most energetically favorable conformation for each ligand was chosen for further analysis. Figures 3 and 4A-6A were generated using the Ligand Interaction Diagram tool of Maestro GUI (38), whereas Figure 4B-6B were prepared using the software PyMOL (42).

The program VolSurf+ (43,44) was used to calculate the physicochemical and ADME properties of the analyzed compounds.

Results and Discussion

Synthesis of pyrazolobenzothiazines 1a-k, 2a-k, and 4-6.

The synthetic pathways utilized in the preparation of the pyrazolobenzothiazines **1a** (45), **1b-k**, **2a** (45), **2b-k** and **4-6** are outlined in Schemes 1 and 2, whilst compounds belonging to the subset **3** (Table 1) were already described and prepared according to the literature (46). N-1 phenylpyrazolobenzothiazines **1a** (45) and **1b-i** were obtained through a regioselective condensation (47) of appropriate phenylhydrazine hydrochloride with the key synthon **7** (30) (Scheme 1). Initially, this reaction step was carried out employing the procedure described for the preparation of derivatives **3** (46), which entails the condensation of intermediate **7** with phenylhydrazines hydrochloride using classical conditions such as EtOH at reflux with traces of H_2SO_4 as dehydrating agent. This procedure suffers from very long time (several days) and moderate to low yields, depending on the utilized substrate. Herein, we report a more advantageously method to obtain compounds **1a-i**. In particular, microwave (MW) irradiation of a mixture of benzothiazine **7** and appropriate phenylhydrazine hydrochloride in

DMF at 100 °C afforded in good yield (60-70%) and very short time (5-75 min) the desired pyrazolobenzothiazines **1a-i**. Target nitro derivative **1i** was then hydrogenated under catalytic conditions to amino derivative **1j**, which was further elaborated to sulfonamidomethyl derivative **1k** by a mesylation reaction.

On the other hand, the target derivatives **2a** (45), **2b-g** and **2i** (Scheme 1) were obtained from **1a-g** and **1i**, respectively by methylation in DMF using MeI and NaH as base.

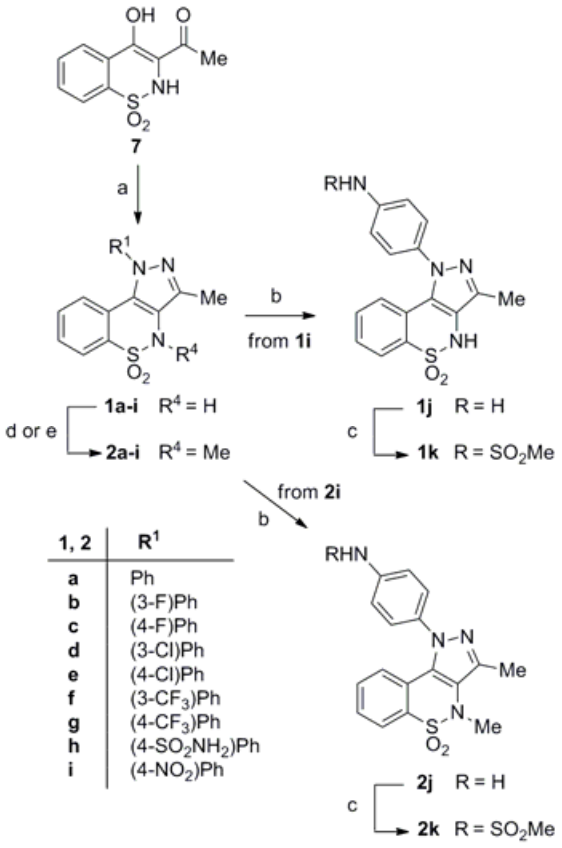

Scheme 1. Synthesis of pyrazolobenzothiazine subsets **1** and **2.** *Reagents and conditions*: a) $ArNH_2NH_2 \cdot HCl$, DMF, 100 °C, MW; b) H_2, Raney-Ni, rt, atm pressure; c) MsCl, CH_2Cl_2/pyridine (1:1), 50 °C; d) MeI, NaH, dry DMF, rt (for **2a-g** and **2i**) or e) MeI, K_2CO_3, dry DMF, rt (for **2h**).

Methylation of compound **1h** to give derivative **2h** was instead realized replacing NaH with K_2CO_3 in order to avoid the formation of exocyclic N-methylated sulfonamide group. In addition, starting from derivative **2i** and employing the same conditions as used for the preparation of **1j** and **1k**, compounds **2j** and **2k** were obtained.

The preparation of target derivatives **4**-**6** (Scheme 2) started from the commercially available saccharin sodium salt, which was reacted with 2-bromo-1-(4-fluorophenyl)ethanone in DMSO at 70 °C to give benzoisothiazole **8** (31) in good yield.

It was then expanded to benzothiazine **9** (31) in EtOH and using NaOEt at 60 °C. Intermediate **9** was reacted with methylhydrazine in EtOH under MW irradiation at 100 °C to give a nearly equimolecular ratio of N-1-methyl- and N-2-methyl-pyrazolobenzothiazine regioisomers **10** and **11**. This mixture resulted very difficult to separate by flash chromatography, so that it was used as is for the methylation reaction. This latter reaction was conducted in DMF in presence of MeI and NaH affording N-4-metylated targets **4** and **5**, respectively, which were separated by flash chromatography. The molecular structure of **4** was in depth analyzed performing a 2D NMR spectrum which showed two diagnostic interactions observed between the H-8 and the H-9 protons of pyrazolobenzothiazine nucleus with the N-1 methyl group. No interactions were found between the N-1 methyl and the H-2' and H-6' of the C-3 phenyl ring (Figure 2).

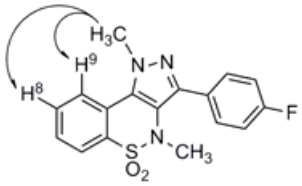

Figure 2. NOESY experiments for **4** showed two main interactions: N-1- Me→H-8 and N-1-Me→H-9.

On the other hand, derivative **9** was also selectively methylated at N-4 position to give intermediate **12** employing a mixture of 1N NaOH/EtOH and MeI at room temperature as reported for similar compounds (48). Finally, intermediate **12** was condensed with hydrazine monohydrate at 70 °C under sonication, following the procedure reported for other pyrazolobenzothiazines (49), to give the target compound **6**.

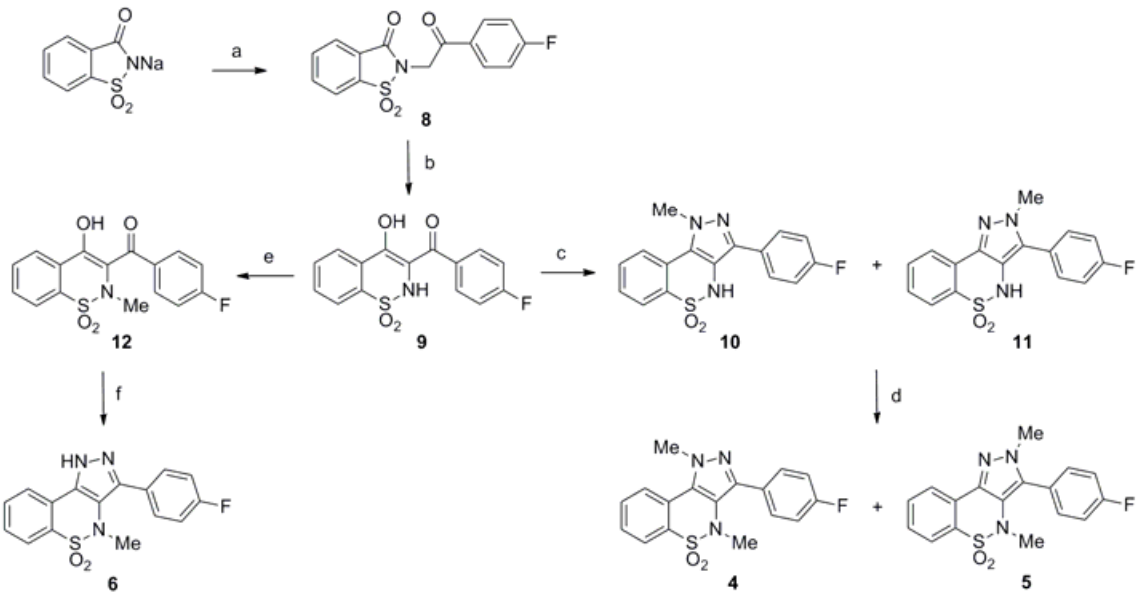

Scheme 2. Synthesis of pyrazolobenzothiazines **4-6**. *Reagents and conditions*: a) $BrCH_2CO(4\text{-}FC_6H_5)$, dry DMSO, 70 °C; b) NaOEt, EtOH, 55 °C; c) $MeNHNH_2$, EtOH, 100 °C, MW; d) MeI, NaH, dry DMF, rt; e) MeI, 1N NaOH, EtOH, rt; f) NH_2NH_2 H_2O, 70 °C, sonication.

Biological evaluation of compounds 1-6

Target compounds **1a-k**, **2a-k**, **3a-c**, **3f-k** and **4-6** were evaluated for their ability to inhibit both p38α MAPK activity and TNF-α release in lipopolysaccharide (LPS) stimulated in human whole blood (HWB), and the results are reported in Table 1.

The biochemical test determines the ability of a compound to compete with ATP for its binding at the p38α MAPK catalytic domain. The phosphorylation of activating transcription factor-2 (ATF-2) was determined with an anti-phospho-ATF-2 antibody. The degree of phosphorylation inversely correlated with the inhibitory activity of the tested compound (32). In this assay, compounds were considered primary actives only when the inhibition of the p38α MAPK phosphorylation activity was reduced at least of 65% employing 10 μM compound concentration. The compounds selected as primary actives were tested in dose response assay to calculate the 50% inhibitory concentration (IC_{50}) values. **SB203580** was included as an internal reference and inhibited p38α MAPK with an IC_{50} value of 0.05 ± 0.001 μM, consistent with previously reported data (25).

The HWB assay was used to determine the anti-inflammatory activity of the tested compounds. This assay is commonly used also because it takes into account the behavior of a compound in the physiological conditions (*e.g.* water solubility at physiological pH, plasma protein binding, cell permeability, ATP concentration, cell metabolism, etc.). Reduction in the

TNF-α release was determined by ELISA method after incubation of HWB with LPS (33). The IC_{50} were determined as the concentration required to reduce of the 50% the TNF-α concentration.

Results from the enzymatic assay confirmed the initial hypothesis that p38α MAPK could be effectively targeted by the pyrazolobenzothiazine chemotype. In fact, derivatives **1d**, **1f**, **1i**, **1k**, **3a**-**c**, **3f**, **3h**, **3i**, **3k**, and **4**-**6** emerged as effective inhibitors with IC_{50} values ranging from 0.43 to 7.73 μM (Table 1).

Table 1. p38α MAPK and TNF-α inhibition of pyrazolobenzothiazines **1**-**6**.

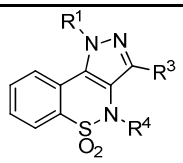

cpds	R_1	R_3	R_4	% inh. p38α[a]	IC_{50} (μM) p38α[b]	IC_{50} (μM) TNF-α HWB[c]
1a		Me	H	26.4	NC[d]	92.3±5.6
1b		Me	H	52	NC[d]	>100
1c		Me	H	46.8	NC[d]	>100
1d		Me	H	91	0.936±0.296	18±3.5
1e		Me	H	24.5	NC[d]	>100
1f		Me	H	74.7	0.967±0.137	>100
1g	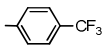	Me	H	41.3	NC[d]	>100
1h	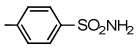	Me	H	60.1	NC[d]	>100
1i	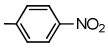	Me	H	67.8	2.784±0.694	>100
1j	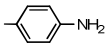	Me	H	30	NC[d]	>100
1k	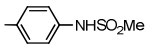	Me	H	85.1	0.593±0.099	20±2.6
2a		Me	Me	14.4	NC[d]	>100
2b		Me	Me	19.5	NC[d]	>100
2c		Me	Me	36.4	NC[d]	>100
2d		Me	Me	27.7	NC[d]	31±1.8

2e		Me	Me	35.6	NC[d]	>100
2f		Me	Me	16.8	NC[d]	>100
2g	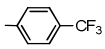	Me	Me	26.6	NC[d]	25±2.1
2h	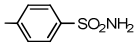	Me	Me	15	NC[d]	>100
2i	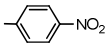	Me	Me	28.2	NC[d]	>100
2j	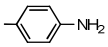	Me	Me	25.5	NC[d]	>100
2k	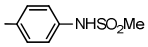	Me	Me	33.9	NC[d]	>100
3a[(46)]			H	65.8	7.727± 1.196	>100
3b[(46)]			H	79.5	2.863±0.169	52±2.5
3c[(46)]			H	87	1.949±0.314	43±2.8
3f[(46)]			H	75.3	3.332±0.168	>100
3g[(46)]	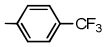		H	51.5	NC[d]	82.7±5.2
3h[(46)]	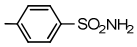		H	78.8	2.749±0.294	>100
3i[(46)]	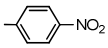		H	76.5	3.529±0.119	51±3.2
3j[(46)]	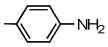		H	50	NC[d]	>100
3k[(46)]	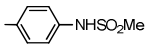		H	81.7	1.124±0.357	32.4±2.8
4	Me		Me	96	0.431±0.053	>100
5	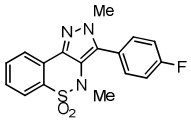			82	2.424±0.154	12±1.8
6	H		Me	95	0.457±0.054	0.5±0.1

[a] The percentage of inhibition was determined employing a 10 μM compound solution and evaluating the phosphorylation state of the ATF-2 substrate. The degree of phosphorylation inversely correlates with the inhibitory activity of the tested compound. Only compounds that were able to inhibit the kinase activity by a percentage ≥ 65% were further analyzed to determine the IC_{50}. [b] IC_{50} represents the compound concentration necessary to reduce by 50% the phosphorylation degree of ATF-2. Data are from three separate experiments±SD. [c] IC_{50} represents the compound concentration required to reduce by 50% the TNF-α levels employing ELISA method. Data are from three separate experiments±SD. [d] NC= not calculated.

The p38α MAPK inhibition data analysis suggested a few SAR trends. Focusing the attention on the subset **1**, it emerged that compounds **1d**, **1f**, **1i**, and **1k**, bearing a N-4 acidic endocyclic sulfonamide function, showed promising activity with IC_{50} values going from 0.59

to 2.78 μM. When this N-4 nitrogen atom was methylated, as in subset **2**, the inhibitory effect on the p38α MAPK activity dramatically decreased (compare **2d**, **2f**, **2i**, and **2k** vs **1d**, **1f**, **1i**, and **1k**, respectively). Overall, derivatives belonging to the subset **2** showed only a very weak effect at 10 μM concentration with percentages of inhibition ranging from 14 to 36. At the same time, with the exception of two compounds, pyrazolobenzothiazines belonging to subset **3** showed good p38α MAPK inhibitory activity. Although they differed for the substituent at C-3 position of the pyrazolobenzothiazine scaffold, compounds of subset **3** had the same acidic sulfonamide feature as in subset **1**, indicating that the presence of the N-4 acidic sulfonamide moiety appears to be very important to ensure p38α MAPK inhibitory activity.

When comparing subsets **1** and **3**, the influence of the substituents placed at C-3 position was not well attributable because either the methyl group or the *para*-chlorophenyl ring gave active compounds. In some cases the presence of the C-3 *para*-chlorophenyl ring permitted a good activity to be recovered with respect to the parent C-3 methyl derivatives of subset **1** (*i.e.* **3a**-**c** and **3h** vs **1a**-**c**, and **1h**, respectively). Independently from the C-3 substituent, the presence of a *meta*-trifluoromethyl, *para*-nitro and *para*-sulfonamidomethyl groups at N-1 phenyl ring granted active compounds in both **1** and **3** subsets.

A different behaviour was observed in subsets **4**-**6** characterized by the absence of the N-1 phenyl ring in the pyrazolobenzothiazine nucleus coupled with the presence of a C-3 *para*-fluorophenyl group and a methyl group at the N-4 position. The good inhibitory activity obtained in the absence of the acidic endocyclic sulfonamide moiety was in contrast with the SAR observed for subsets **1-3**. This distinctive behaviour suggested that pyrazolobenzothiazines **4**-**6** could present different interacting residues and/or binding modes within the p38α MAPK ATP binding site compared to derivatives of subsets **1** and **3**. It is worth noting that compounds **4** and **6** displayed the best IC_{50} values among the whole set of pyrazolobenzothiazine derivatives.

The HWB assay revealed that derivative **6** showed the best activity, with an IC_{50} value of 0.5 μM, in perfect agreement with its p38α inhibition potency. Although derivatives **1d**, **1k**, **3b**, **3c**, **3i**, **3k** and **5** exhibited promising inhibitory activity in the p38α MAPK assay, they were only moderately active in reducing TNF-α release (HWB assay). Additionally, no correlation was observed between the potency obtained in the enzyme and in the TNF-α release assays for compounds **1f**, **1i**, **3a**, **3f**, **3h**, and **4.** This behaviour could be explained either by the relative low potency of some compounds in p38α MAPK assay or by considering that the HWB assay differs from the *in vitro* enzyme assay by additional factors, such as plasma protein binding, cell permeability, ATP concentration, various cell types and possible metabolism, all influencing heavily the activity of the tested compounds in cells. The results of the HWB assay also demonstrated that compounds **2d** and **2g** were moderate inhibitors

of TNF-α release. The absence of activity of these two derivatives against the isolated p38α suggested that other targets are probably involved in their ability to block TNF-α production.
Overall, the data indicated derivative **6** (IC_{50}s of 0.457 μM and 0.5 μM on biochemical and HWB assays, respectively) as effective p38α MAPK inhibitor within the explored series of pyrazolobenzothiazines. Although compound **6** was less potent than **SB203580**, it turned out to be an efficient inhibitor, as highlighted by the corresponding ligand efficiency (LE) and lipophilic efficiency (LipE) values (Table 2). In fact, derivative **6** had LE value greater than 0.3, that is the generally accepted lower limit of efficiency in lead discovery and optimization. Moreover, although LipE greater than 5 is usually considered optimal for a promising drug candidate, mean LipE values of 2.5 and 3.6 have been reported for collection of HTS hits and leads, respectively (50).

Table 2. LE values, and predicted LipE, physicochemical and ADME parameters

Cpds	LE[a]	LipE[b]	MW[c]	PSA[d]	LgD7.5[e]	LgS7.5[f]	PB[g]	CACO2[h]	MetStab[i]
SB203580	0.37	4.1	377.4	80.2	3.2	-5.2	92.8	0.7	47.1
6	0.38	3.4	329.3	75.2	3.0	-3.9	74.4	0.8	57.0

[a] LE: ligand efficiency in units of $kcalmol^{-1}$/heavy atom. LE= $1.4pIC_{50}/N$; N is the number of heavy atoms (27 for **SB203580** and 23 for **6**, respectively) [b] LipE = pIC_{50} – predicted logD7.5. [c] MW: molecular weight. [d] PSA: polar surface area. [e] LgD7.5: logarithm of the octanol/water partition coefficient at pH=7.5. [f] LgS7.5: logarithm of the aqueous solubility at pH=7.5 [g] PB: % of plasma protein binding. [h] CACO2: Caco-2 cell (human intestinal epithelial cell line derived from a colorectal carcinoma) permeability. This value is qualitative, and the compounds are classified in penetrating (CACO2+) or having little if any ability to penetrate the epithelial cells (CACO2-). [i] MetStab is the percentage of the remaining compound after incubation with human CYP3A4 enzyme. Values greater than 50 indicate stable behaviour.

It is also worth noting that the emerged hit compound showed satisfactory in silico determined physicochemical and ADME properties (43,44), comparable to those of the reference compound **SB203580** (Table 2); this analysis further validated compound **6** as a good starting point for future hit-to-lead optimization work.
Based on the results of the biological evaluations, the next step of this research included computational studies aimed at both suggesting a plausible binding mode for this new class of inhibitors and providing some insights to support the SAR analysis. The *in silico* results are reported in the following section.

Binding Mode Analysis

Compound **SB203580** is the prototype of the class of p38α MAPK pyridinylimidazole inhibitors, which have been shown to act as ATP-competitors (28). Crystal structures of

SB203580 bound to p38α MAPK showed that the pyridine ring of the inhibitor occupied the adenine-binding region, with the nitrogen atom accepting a hydrogen bond from the NH backbone of Met109 in the hinge region (residues 106-110) (35,51-53) (Figure 3). The ligand imidazole core showed π-π interaction with Phe169, with its N-3 atom interacting with the Lys53 side chain. The *para*-fluorophenyl ring was buried into the hydrophobic region I (HRI), which is mainly defined by residues Ala51, Leu75, Iso84, Leu86, Val105, Leu104 and Thr106. Of note, the small gatekeeper residue Thr106 in p38α MAPK provides access to this pocket, thus playing a key role in kinase inhibitor selectivity, as related kinases possess bulkier residue at the same position.

Finally, the *para*-methylsulfinylphenyl group occupied the phosphate-binding region, with the phenyl ring making π-π interaction with Tyr35 (Figure 3).

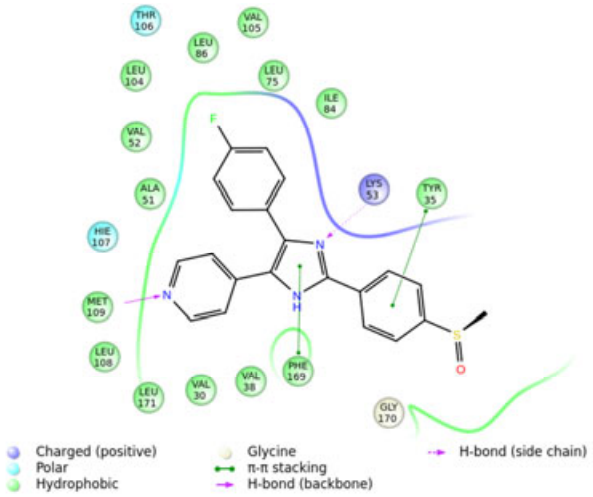

Figure 3. Schematic representation of the interactions between the pyridinylimidazole inhibitor **SB203580** and p38α MAPK ATP binding site (PDB ID 3ZS5 as representative complex). Protein residues lying within a distance of 4 Å from the bound ligand are shown.

Based on the results of the biological evaluations, the most interesting pyrazolobenzothazine derivatives (*i.e.*, **1d**, **1k**, **3k**, and **6**) were selected to investigate the possible ligand-p38α MAPK interactions by means of automated docking experiments. The N-4-methylated inactive derivatives **2d** and **2k** were analysed as well to try to explain the key role of the N-4 acidic sulfonamide moiety in subset **1** compared to subset **2**.

Self-docking calculations of **SB203580** reproduced the experimental binding conformation (RMSD equal to 0.5 Å) as a single solution (100 conformations in one cluster), confirming the good performance of the AutoDock 4.2 software; notably, the predicted inhibition

constant ($K_{i\text{-}pred}$) value (0.024 μM) was in perfect agreement with the experimental IC_{50} value (0.05 μM).

The docking poses of **1d** ($K_{i\text{-}pred}$=0.3 μM) and **1k** ($K_{i\text{-}pred}$=4 μM) were comparable and perfectly aligned to **SB203580**, as shown in Figure 4 using **1d** as representative compound. Similarly to the imidazole core of the known inhibitor, the pyrazole nucleus was able to establish a hydrogen-bonding with Lys53 and stacking interaction with the phenyl side chain of Phe169. Key intermolecular interactions were also identified between the inhibitor *meta*-chlorophenyl moiety and HRI residues.

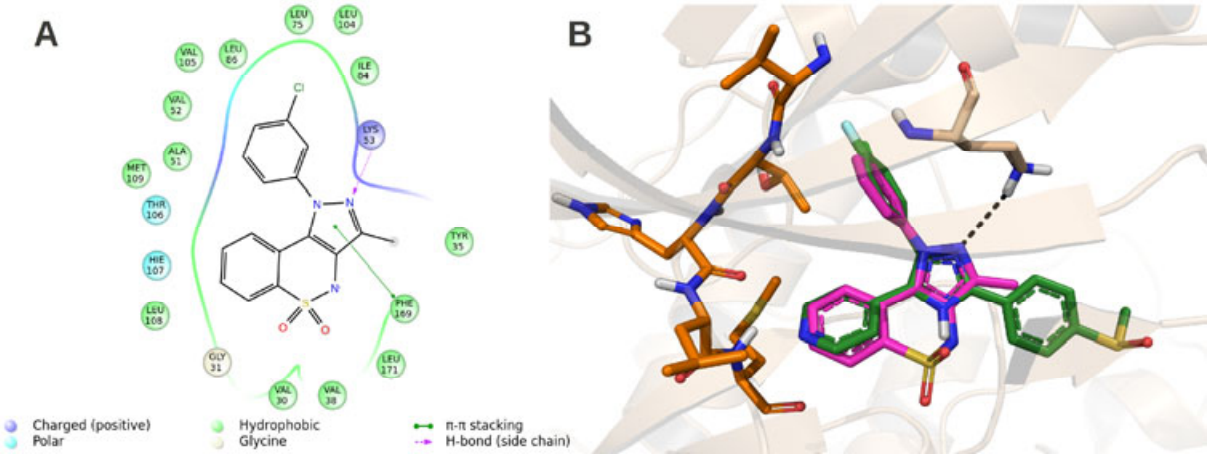

Figure 4. (A) Simplified 2D representation of the predicted interactions between derivative **1d** and the p38α MAPK ATP binding site. (B) Docking pose of compound **1d** (violet) together with the experimental position of **SB203580** (green). The hinge region (orange) and the residues (wheat) establishing hydrogen bond interactions (black dashed lines) with the ligand are highlighted.

The docking results for the inactive N-methylated derivatives **2d** and **2k** suggested that the presence of a methyl group at N-4 position could prevent these compounds by establishing the crucial intermolecular interactions needed to inhibit p38α MAPK enzymatic activity. In fact, compounds **2d** and **2k** only partially occupied the ATP-binding site, and differently from subset **1**, they lacked the key interactions with residues defining HRI (see Supporting Information).

The Autodock-conformation of active compound **3k** ($K_{i\text{-}pred}$=0.71 μM, Figure 5) was somewhat similar to that of **SB203580,** but different with respect to the one observed for the subset **1**. In fact, whilst in the latter compounds the HRI was occupied by the phenyl substituent at the N-1 position, in subset **3** this hydrophobic pocket accommodated the *para*-chlorophenyl substituent at the C-3 position, which also showed π-cation interaction with

Lys53. Furthermore, one of the sulfone oxygen atoms served as H-bond acceptor to the main chain nitrogen of the hinge region residue Met109 in a manner analogous to the pyridine nitrogen of the known p38α MAPK inhibitor **SB203580**, whereas the pyrazole ring established aromatic stacking interaction with Phe169. An additional polar contact was engaged between the exocyclic sulfonamide fragment and the nitrogen atom of the Gly170 backbone.

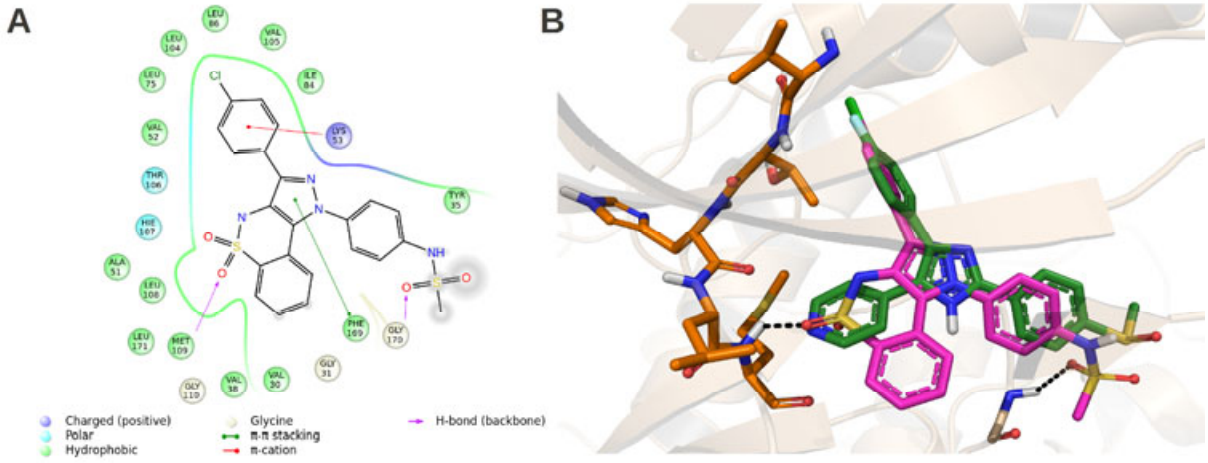

Figure 5. (A) Schematic representation of the predicted interactions between compound **3k** and the p38α MAPK residues. (B) Predicted binding mode of **3k** (violet) into the ATP binding site. Experimental position of **SB203580** is depicted in green sticks as reference. Intermolecular hydrogen bonds are shown as black dashed lines, whereas the hinge region is illustrated in orange.

Finally, the docking solutions for the two tautomers of **6** showed a conserved ligand pose superimposable to that observed for derivative **3k** (Figure 6). In particular, one of the sulfone oxygens of the ligand interacted with Met109, the *para*-fluorophenyl group was located in the HRI, and the pyrazole ring formed a stacking interaction with Phe169. Similarly to the N-3 atom of the **SB203580** imidazole nucleus, the N-2 atom of 1H-pyrazole tautomer of derivative **6** ($K_{i\text{-}pred}$=0.67 μM) formed an anchoring H-bond with Lys53; this contact could not be observed in the docking conformation of 2H-pyrazole tautomer ($K_{i\text{-}pred}$=1.89 μM) where the same nitrogen atom was protonated.

Interestingly, the lack of interaction with Lys53 might be also responsible of the lower activity of the N-2-methylated derivative **5** (IC_{50}=2.43 μM) compared to the strict N-unsubstituted analogue **6** (IC_{50}=0.455 μM) (see Supporting Information).

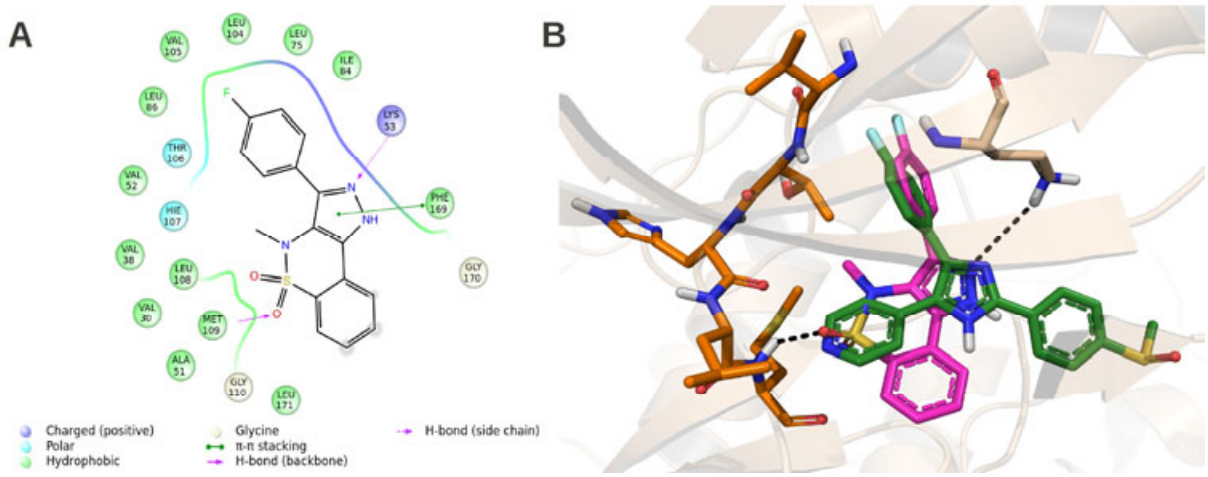

Figure 6. (**A**) Simplified 2D representation of the predicted interactions between derivative **6** (tautomer 1H-pyrazole as example) and the p38α MAPK residues. (**B**) Docking pose of compound **6** (violet) together with the experimental position of **SB203580** (green). Residues defining the hinge region are shown in orange, while the hydrogen bonds are represented as dashed black lines.

Kinase selectivity assessment

Spurred by the interesting biological results and with the aim to further validate the potential of the pyrazolobenzothiazines as a new class of p38α-MAPK inhibitors, we decided to evaluate the best compounds **1d** and **6** against a panel of 14 kinases available in our hands (Table 3). This hit verification assay is critical for highlighting potential undesirable side effects due to the inhibition of other kinases, thus leading to the identification of potential off-targets.

Data from inhibition of other MAPKs showed that compounds **1d** and **6** did not inhibit Erk1, p38δ and p38γ, whereas they were able to block the catalytic activity of p38β. These results could be explained considering that, differently from p38α and p38β, the other three MAPKs show a gatekeeper residue larger than Thr, which could prevent the accommodation of the meta-chlorophenyl (**1d**, Figure 4) and para-fluorophenyl (**6**, Figure 6) rings in a suitable hydrophobic region. Interestingly, derivatives **1d** and **6** did not inhibit the activity of structurally distinct CDC2, CDK5, JAK2, LCK, SRC, and PKAC-α kinases. Among all the

kinases evaluated, only JAK3 seemed to be significantly inhibited by compound **1d**. On the contrary, derivative **6** was unable to inhibit the same kinase over 70% at 100 μM. A weak activity was instead observed for both derivatives against PDGFRb and GSK3-β kinases, although no complete inhibition of the enzymatic activity was observed.

Overall, we can conclude that derivative **6** has a reasonable kinase selectivity profile within the explored set of kinases.

Table 3. Kinase selectivity profile of derivatives **1d** and **6**

kinase	**1d**		**6**	
	%inh. @100 μM[a]	IC_{50} (μM)[b]	%inh. @100 μM[a]	IC_{50} (μM)[b]
CDC2	21±1	ND	27±3	ND
CDK5	23±1	ND	30±4	ND
Erk1	30±1	ND	20±4	ND
JAK2	33±1	ND	23±3	ND
JAK3	79±5	2.5[c]	52±1	ND
LCK	1±1	ND	2±2	ND
SRC	6±1	ND	3±2	ND
p38-β	100±2	16	100±2	1.7
p38-δ	22±3	ND	25±1	ND
p38-γ	51±1	ND	13±1	ND
PDGFRb	82±2	82.9[c]	100±1	58.1[c]
GSK3-β	74±4	24.9[c]	78±3	48.4[c]
PKAC-α	7±2	ND	26±4	ND

[a] a dose-response curve was generated only for compounds reaching 70% inhibition of kinase activity. [b] IC_{50} represents the concentration required to reduce by 50% the kinase activity expressed as the ability to phosphorylate a specific substrate in presence of ATP. [c] The compound does not completely inhibit the enzymatic activity. IC_{50} value extrapolated by the analysis software might be not accurately estimated.

Conclusion and future directions

The availability of in-house pyrazolobenzothiazine-based compounds led to the identification of a novel chemical series of p38α MAPK inhibitors.

Some pyrazolobenzothiazines exhibited promising biological activity in both enzyme and HWB assays, with **6** resulting the most potent compound. The low molecular weight, ligand efficiency values and kinase selectivity profile of pyrazolobenzothiazine **6** make this derivative an attractive starting point for chemistry efforts aimed at further potency

optimization. For instance, it is well known that the potency and selectivity of a moderate p38α inhibitor can be improved by establishing additional interactions with the less-conserved solvent-exposed front region (hydrophobic region II) of the protein (23). Therefore, taking into account the above-described binding mode, we figure it could be possible to optimize the hit compound **6** by adding suitable substituents on the phenyl ring of the pyrazolobenzothiazine scaffold.

Acknowledgements

We are grateful to Dr. Davide Martino for assisting with HWB assay and to Dr. Nunzio Iraci for technical assistance in computational studies and critical reading of the manuscript.

References

1. Schieven, G. L. (2005) The biology of p38 kinase: a central role in inflammation. Curr Top Med Chem 5: 921-928.
2. Saklatvala, J. (2004) The p38 MAP kinase pathway as a therapeutic target in inflammatory disease. Curr Opin Pharmacol 4: 372-377.
3. Feng, Y. J. Li, Y. Y. (2011) The role of p38 mitogen-activated protein kinase in the pathogenesis of inflammatory bowel disease. J Dig Dis 12: 327-332.
4. Patterson, H. Nibbs, R. McInnes, I. Siebert, S. (2014) Protein kinase inhibitors in the treatment of inflammatory and autoimmune diseases. Clin Exp Immunol 176: 1-10.
5. Wang, G. Pan, J. Chen, S. D. (2012) Kinases and kinase signaling pathways: potential therapeutic targets in Parkinson's disease. Prog Neurobiol 98: 207-221.
6. Namiki, K. Matsunaga, H. Yoshioka, K. Tanaka, K. Murata, K. Ishida, J. Sakairi, A. Kim, J. Tokuhara, N. Shibakawa, N. Shimizu, M. Wada, Y. Tokunaga, Y. Shigetomi, M. Hagihara, M. Kimura, S. Sudo, T. Fukamizu, A. Kasuya, Y. (2012) Mechanism for p38α-mediated experimental autoimmune encephalomyelitis. J Biol Chem 287: 24228-24238;
7. Krementsov, D. N. Thornton, T.M. Teuscher, C. Rincon, M. (2013) The emerging role of p38 mitogen-activated protein kinase in multiple sclerosis and its models. Mol Cell Biol 33: 3728-3734.
8. Xu, Y. Li, N. Xiang, R. Sun, P. (2014) Emerging roles of the p38 MAPK and PI3K/AKT/mTOR pathways in oncogene-induced senescence. Trends Biochem Sci 39: 268-276.

9. Hong, B. Li, H. Zhang, M. Xu, J. Lu, Y. Zheng, Y. Qian, J. Chang, J. T. Yang, J. Yi, Q. (2014). p38 MAPK inhibits breast cancer metastasis through regulation of stromal expansion. Int. J. Cancer. doi: 10.1002/ijc.28958.
10. Koul, H. K. Pal, M. Koul, S. (2013) Role of p38 MAP Kinase Signal Transduction in Solid Tumors**.** Genes Cancer 4: 342-359.
11. Zhou, W. Hu, W. (2013) Anti-neuroinflammatory agents for the treatment of Alzheimer's disease. Future Med Chem 5: 1559-1571.
12. Munoz, L. Ammit, A. J. (2010) Targeting p38 MAPK pathway for the treatment of Alzheimer's disease. Neuropharmacology 58: 561-568.
13. Coulthard, L. R. White, D. E. Jones, D. L. McDermott, M. F. Burchill, S. A. (2009) p38(MAPK): stress responses from molecular mechanisms to therapeutics. Trends Mol Med 15: 369-379
14. Cuadrado, A. Nebreda, A. R. (2010) Mechanisms and functions of p38 MAPK signaling. Biochem J 429: 403-417.
15. Kumar, S. Boehm, J. Lee, J. C. (2003) p38 MAP kinases: key signaling molecules as therapeutic targets for inflammatory diseases. Nature Rev Drug Discov 2: 717-726.
16. Wroblesky, S. T. Doweyko, A. M. (2005) Structural comparison of p38 inhibitor-protein complexes: a review of recent p38 inhibitors having unique binding interactions. Curr Top Med Chem 5: 1005-1016.
17. Wagner, G. Laufer, S. (2006) Small molecular anti-cytokine agents. Med Res Rev 26: 1-62.
18. Margutti, S. Laufer, S. A. (2007) Are MAP kinases drug targets? Yes, but difficult ones**.** ChemMedChem 2: 1116-1140.
19. Goldestein, D. M. Kuglstatter, A. Lou, Y. Soth, M. J. (2010) Selective p38alpha inhibitors clinically evaluated for the treatment of chronic inflammatory disorders. J Med Chem 53: 2345-2353.
20. Schnieders, M. J. Kaoud, T. S. Yan, C. Dalby, K. N. Ren, P. (2012) Computational insights for the discovery of non-ATP competitive inhibitors of MAP kinases. Curr Pharm Des 18: 1173-1185.
21. Kong, T.-T. Zhang, C-M. Liu, Z.-P. (2013) Recent developments of p38α MAP kinase inhibitors as antiinflammatory agents based on the imidazole scaffolds. Curr Med Chem 20: 1997-2016.
22. https://clinicaltrials.gov/ct2/results?term=p38&Search=Search (accessed September, 12, 2014).
23. Bühler, S. Laufer, S. A. (2014) p38 MAPK inhibitors: a patent review (2012-2013). Expert Opin Ther Patents 24: 1-20.

24. Cecchetti, V. Fravolini, A. Schiaffella, F. De Regis, M. Orzalesi, G. Volpato, I. (1983) Synthesis and Pharmacological Activity of Pyrazolo-1,2-benzothiazine- and Isoxazolo-1,2-benzothiazinecarboxamides. Il Farmaco 38: 35–44.

25. Gallagher, T. F. Seibel, G. L. Kassis, S. Laydon, J. T. Blumenthal, M. J. Lee, J. C. Lee, D. Boehm, J. C. Fier-Thompson, S. M. Abt, J. W. Soreson, M. E. Smietana, J. M. Hall, R. F. Garigipati, R. S. Bender, P. E. Erhard, K. F. Krog, A. J. Hofmann, G. A. Sheldrake, P. L. McDonnell, P. C. Kumar, S. Young, P. R. Adams, J. L. (1997) Regulation of stress-induced cytokine production by pyridinylimidazoles; inhibition of CSBP kinase. Bioorg Med Chem 5: 49-64.

26. Cuenda, A. Rouse, J. Doza, Y. N. Meier, R. Cohen, P. Gallagher, T. F. Young, P. R. Lee, J. C. (1995) SB 203580 is a specific inhibitor of a MAP kinase homologue which is stimulated by cellular stresses and interleukin-1. FEBS Letters 364: 229-233.

27. Tong, L. Pav, S. White, D. M. Rogers, S. Crane, K. M. Cywin, C. L. Brown, M. L. Pargelli, C. A. (1997) A highly specific inhibitor of human p38 MAP kinase binds in the ATP pocket. Nat Struct Biol 4: 311-316.

28. Young, P. R. McLaughlin, M. M. Kumar, S. Kassis, S. Doyle, M. L. McNulty, D. Gallagher, T. F. Fisher, S. McDonnel, P. C. Carr, S. A. Huddleston, M. J. Seibel, G. Porter, T. G. Livi, G. P. Adams, J. L. Lee, J. C. (1997) Pyridinyl imidazole inhibitors of p38 mitogen-activated protein kinase bind in the ATP site. J Biol Chem 272: 12116-12121.

29. Gum, R. J. McLaughlin, M. M. Kumar, S. Wang, Z. Bower, M. J. Lee, J. C. Adams, J. L. Livi, G. P. Goldsmith, E. J. Young, P. R. (1998) Acquisition of sensitivity of stress-activated protein kinases to the p38 inhibitor, SB 203580, by alteration of one or more amino acids within the ATP binding pocket. J Biol Chem 273: 15605-15610.

30. Zinnes, H. Comes, R. A. Zulesky, F. R. Caro, A. N. Shavel, J. Jr. (1965) 1,2-Benzothiazines. II. The preparation and sodium borohydride reduction of 3-acyl-2H-1,2-benzothiazin-4(3H)-one 1,1-dioxides. J Org Chem 30: 2241-2246.

31. Hasegawa, T. Motoizumi, M. Kobayashi M (Sankyo, Co, Ltd, Japan) (2007) Benzothiadiazine derivatives. Japanese Pat. JP 2007197369A.

32. Goettert, M. Graeser, R. Laufer, S. A. (2010) Optimization of a nonradioactive immunosorbent assay for p38alpha mitogen-activated protein kinase activity. Analyt Biochem 406: 233-234.

33. Koch, P. Baeuerlein, C. Jank, H. Laufer, S. (2008) Targeting the ribose and phosphate binding site of p38 mitogen-activated protein (MAP) kinase: synthesis and biological testing of 2-alkylsulfanyl-, 4(5)-aryl-, 5(4)-heteroaryl-substituted imidazoles. J Med Chem 51: 5630-5640.

34. Morris, G. M. Huey, R. Lindstrom, W. Sanner, M. F. Belew, R. K. Goodsell, D. S. Olson, A. J. (2009) Autodock4 and AutoDockTools4: automated docking with selective receptor flexiblity. J Comput Chem 16: 2785-91.

35. Azevedo, R. van Zeeland, M. Raaijmakers, H. Kazemier, B. de Vlieg, J. Oubrie, A. (2012) X-ray structure of p38α bound to TAK-715: comparison with three classic inhibitors. Acta Cryst D68: 1041-1050.

36. Protein Preparation Wizard 2013-3; Epik version 2.4, Schrödinger, LLC, New York, NY, 2013; Impact version 5.9, Schrödinger, LLC, New York, NY, 2013; Prime version 3.2, Schrödinger, LLC, New York, NY, 2013.

37. Sastry, G. M. Adzhigirey, M. Day, T. Annabhimoju, R. Sherman, W. (2013) Protein and ligand preparation: parameters, protocols, and influence on virtual screening enrichments. J Comput Aided Mol Des 27: 221-234.

38. Maestro, version 9.6; Schrödinger, LLC: New York, NY, 2013.

39. Milletti, F. Storchi, L. Sforna, G. Cruciani, G. (2007) New and original pKa prediction method using grid molecular interaction fields. J Chem Inf Model 47: 2172–2181.

40. Cruciani, G. Milletti, F. Storchi, L. Sforna, G. Goracci, L. (2009) In silico pKa prediction and ADME profiling. Chem Biodivers 6:1812–1821.

41. Sanner, M. F. (1999) Python: a programming language for software integration and development. J Mol Graphics Mod 17: 57-61

42. The PyMOL Molecular Graphics System, version 1.5.0.4; Schrödinger, LLC: New York, 2013.

43. VolSurf+. http://www.moldiscovery.com/software/vsplus

44. Cruciani, G. Crivori, P. Carrupt, P. A. Testa, B. Molecular fields in quantitative structure–permeation relationships: the VolSurf approach. (2000) J Mol Struct (Theochem) 503: 17–30.

45. Shavel, J. Jr. Zinnes H. (1967) Pyrazolo [4,3-*c*] [1,2] benzothiazine 5, 5-dioxides and process for their production (Warner-Lambert Pharmaceutical Co; Rockaway, New Jersey, USA), US Pat. US 3346572.

46. Sabatini, S. Gosetto, F. Serritella, S. Manfroni, G. Tabarrini, O. Iraci, N. Brincat, J. P. Carosati, E. Villarini, M. Kaatz, G.W. Cecchetti, V. (2012) Pyrazolo[4,3-*c*][1,2]benzothiazines 5,5-dioxide: a promising new class of Staphylococcus aureus NorA efflux pump inhibitors. J Med Chem 55: 3568-3572.

47. Barreca, M. L. Manfroni, G. Leyssen, P. Winquist, J. Kaushik-Basu, N. Paeshuyse, J. Krishnan, R. Iraci, N. Sabatini, S. Tabarrini, O. Basu, A. Danielson, U. H. Neyts, J. Cecchetti, V. (2013) Structure-based discovery of pyrazolobenzothiazine derivatives as inhibitors of hepatitis C virus replication. J Med Chem 56: 2270-2282.

48. Shapira, C. B. Perillo, I. A. (1993) 13C NMR Analysis of some 4-hydroxy-2H-1,2-benzothiazine 1,1-dioxides. J Het Chem 30: 1051–1056.

49. Ahmad, M. Siddiqui, H. L. Zia-ur-Rehman, M. Parvez, M. (2010) Anti-oxidant and anti-bacterial activities of novel N'-arylmethylidene-2-(3, 4-dimethyl-5, 5-dioxidopyrazolo[4,3-c][1,2]benzothiazin-2(4H)-yl) acetohydrazides. Eur J Med Chem 45: 698-704.

50. Tarcsay, A. Nyiri, K. Keserű, G. M. (2012) Impact of Lipophilic Efficiency on Compound Quality. J Med Chem 55: 1252–1260.

51. Simard, J. R. Getlik, M. Grütter, C. Pawar, V. Wulfert, S. Rabiller, M. Rauh, D. (2009) Development of a fluorescent-tagged kinase assay system for the detection and characterization of allosteric kinase inhibitors. J Am Chem Soc 131: 13286–13296.

52. Wang, Z. Canagarajah, B. J. Boehm, J. C. Kassisà, S. Cobb, M. H. Young, P. R. Abdel-Meguid, S. Adams, J. L. Goldsmith, E. J. (1998) Structural basis of inhibitor selectivity in MAP kinases. Structure 6: 1117-1128.

53. Bukhtiyarova, M. Karpusas, M. Northrop, K. Namboodiri, H. V. M. Springman, E. B. (2007) Mutagenesis of p38alpha MAP kinase establishes key roles of Phe169 in function and structural dynamics and reveals a novel DFG-OUT state. Biochemistry 46: 5687–5696